Reflected shock tunnel noise control

H. G. Hornung and N. J. Parziale

Graduate Aerospace Laboratories, California Institute of Technology

1   Introduction

A reflected shock tunnel is a facility for generating high speed flows by converting the high thermal energy in a hot reservoir into ordered kinetic energy of flow by means of an expansion through a nozzle. The gas in the reservoir reaches its high temperature and pressure by being processed, first by an incident shock and then by the reflection of this shock from the end of a shock tube. The end wall of the shock tube has a central hole that serves as the nozzle throat. It is initially blocked by a weak diaphragm that breaks almost instantaneously at shock reflection.

The presence of the hole causes the shock to be reflected in a manner that is illustrated by the example of a computed flow in Fig. 1. Part of the reflected shock propagates toward the tube axis where it
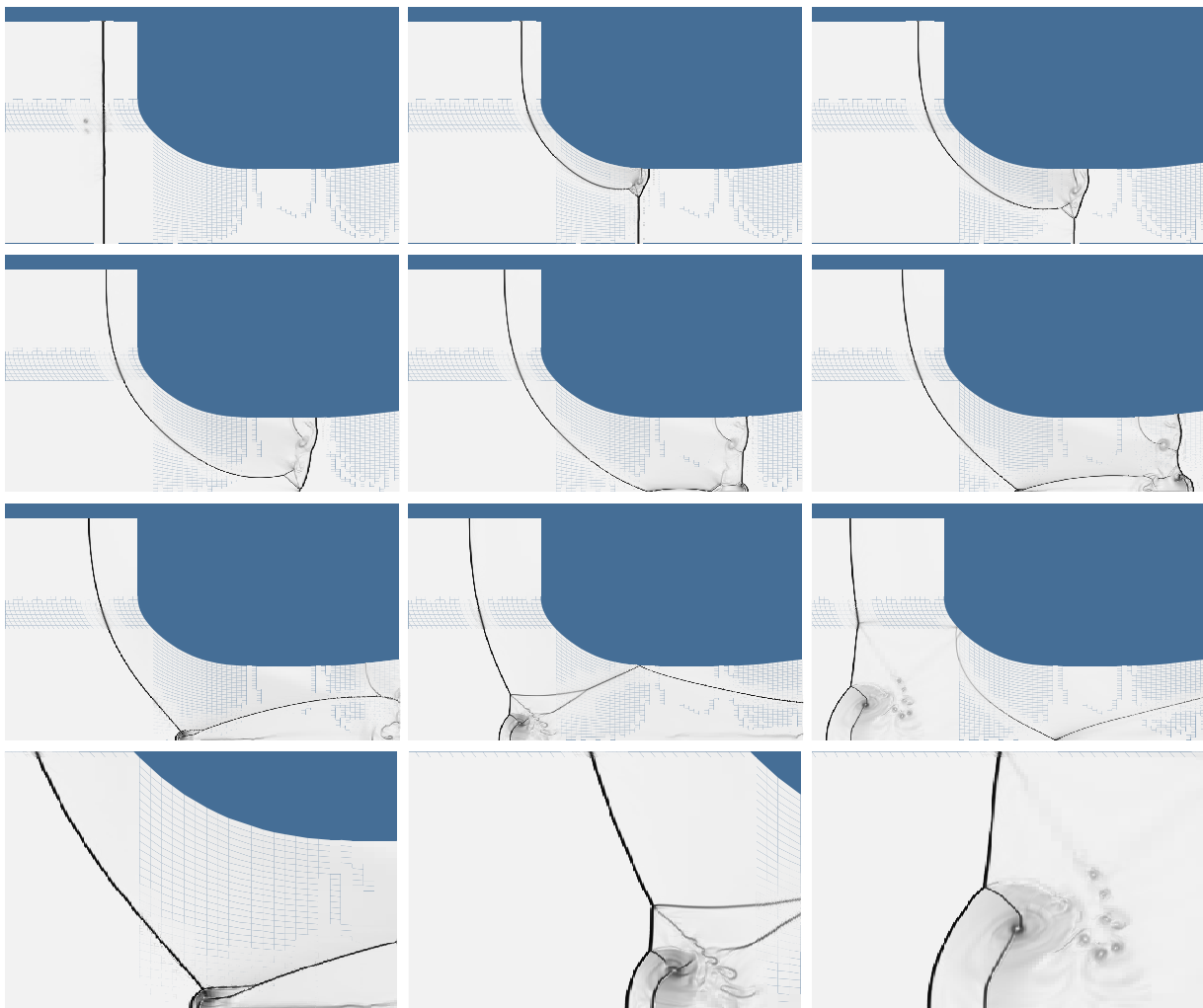

Figure 1: Sequence of pseudo-schlieren images of the reflection of a shock wave from the end of a shock tube equipped with a throat (taken from Hornung, 2000). The shock tube axis is along the bottom edge of the images. Note how the reflected shock is refracted and focused onto the tube axis. The extreme pressure at this reflection from the axis causes structures to be formed that include a strong vortex ring. Parts of the last three frames (third row) are enlarged in the fourth row. The computation solves the Euler equations in a body–fitted grid of 14400 coarse cells with two tiers of adaptive mesh refinement by a factor of 3 each, so that the effective number of cells is 1166400.

reflects toward the tube wall. It may be expected that such a radially propagating shock wave in the shock tube will continue to travel back and forth between the tube wall and axis and thus contribute a substantial amount of noise in the nozzle flow downstream of the throat. As Hornung (2000) showed, placing a rod along the axis to avoid the extreme pressures during reflection from the axis, reduces the severity of the process considerably.

Another problem of shock tunnel operation is that fine debris breaks off the stainless–steel primary diaphragm. This is the diaphragm that initially separates the helium/argon driver gas from the test gas in the shock tube. When this diaphragm bursts and generates the primary shock, very small scale debris is produced that can damage a model placed in the test section. The surface of such models occasionally appears as if it has been sand–blasted. In order to avoid such damage, many shock tunnels place a central body upstream of the throat opening. Diaphragm debris is deflected by such a body and strikes the shock tube end wall, where it is embedded in the copper lining.

Our aim is to examine the possibility of shaping a debris blocker in such a way that we achieve both debris catching and noise reduction. We do this by making unsteady Euler computations of the shock tube and nozzle flows with various configurations.

The field of very high speed flow is, of course, one of the specialties of Academician Vasiliy Fomin, and we dedicate this work to him on the occasion of his 70th birthday.

2   Computation of shock tunnel

2.1   Computational System

For the computations the software system Amrita, constructed by James Quirk, see Quirk (1992), was used. Amrita is a system that automates and packages computational tasks in such a way that the packages can be combined (dynamically linked) according to instructions written in a high–level scripting language. The present application uses features of Amrita that include the automatic construction of different Euler solvers, automatic documentation of the codes, automatic adaptive mesh refinement according to simply chosen criteria, and scripting–language–driven computation, archiving and post–processing of the results. The automation of the assembly and sequencing of the tasks makes for dramatically reduced possibility of hidden errors. More importantly, it makes computational investigations transparent and testable by others. The ability to change one package at a time, without changing the rest of the scheme, permits easy detection of sources of error. The scope of the software system far exceeds its use here. The Euler solver generated for the present computations was an operator–split scheme with HLLE flux and kappa-MUSCL reconstruction.

2.2   T5 shock tunnel without blocker

The T5 hypervelocity shock tunnel has a free–piston driver. The heavy piston heats the helium/argon driver gas by adiabatic compression, thus enabling very high shock speeds to be generated in the shock tube. The shock tube has a diameter of 90 mm and its end is fitted with a throat of 30 mm diameter followed by a nozzle which, in our computations, is conical with a half–angle of 7 °. To simplify matters, the computation is made with a diatomic perfect gas, and the incident shock Mach number in all cases is 10. The computations are made in a Cartesian grid and the solid walls of the facility are specified with a level set that is zero at the solid boundary and measures the closest distance to the wall elsewhere.

The initial condition for the computation is taken at the point when the incident shock is close to the

end wall of the shock tube. At a small distance downstream of the throat the diaphragm separating the low pressure in the nozzle and the test–gas pressure in the shock tube is represented by a discontinuity. This condition is shown in Fig. 2.
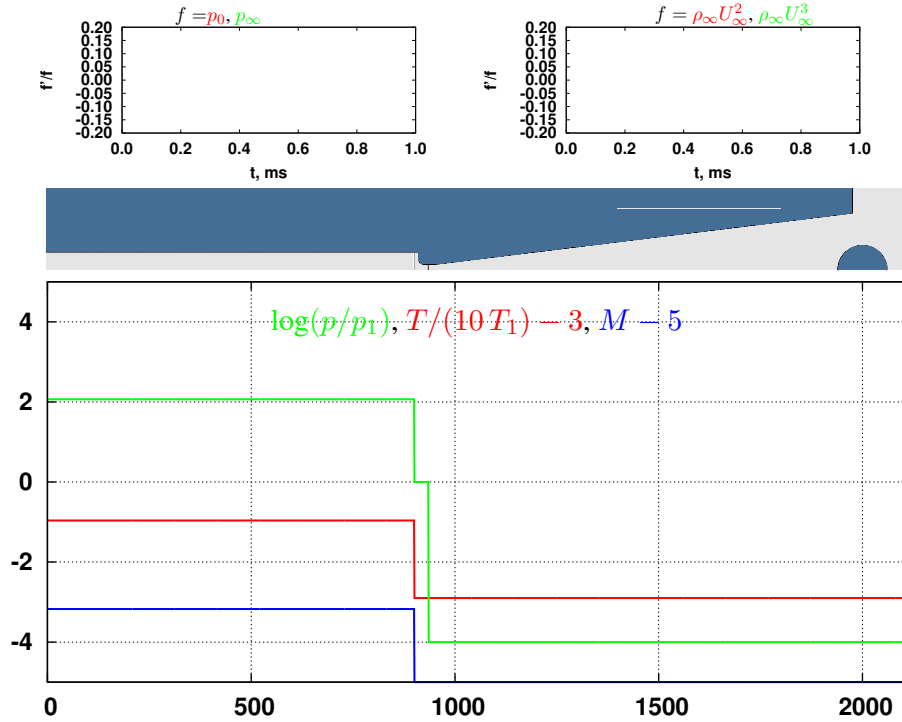

Figure 2: Initial conditions for the computation, showing a pseudo-schlieren image, and plots of pressure, temperature and Mach number in suitable forms along the facility axis. At the left is the shock tube showing a shock wave just before striking the end wall of the tube and a pressure discontinuity just downstream of the throat. As may be seen, the pressure ratio across the shock is just above 100 and the pressure ratio across the diaphragm is 10000. A sphere is placed in the test section for good measure. The scale on the abscissa is in mm.

Fig. 3 shows the situation after running the computation for 11000 time steps. The distributions of the flow quantities show a distinctive dip about half–way along the nozzle. This is a feature of the shape of the throat, which causes a weak shock to be generated at the axis near the throat. this reflects from the nozzle wall and focuses onto the axis, where the distribution is measured. However, the more serious feature is the noise. The traces at the top show that, because p_0 is measured off axis, it is much less noisy than the other traces. The delay between the onset of the red p_0 trace and the green p_∞ trace is the time it takes for the shock to travel between the reservoir and the test section. The starting process of the nozzle takes approximately 500 μs, so the traces end during the first portion of the test time, which is usually around 1 to 2 ms.

The traces show that the typical noise level on the axis of the test section is of the order of $\pm 10\%$. Of course, this is a nominally inviscid flow, and the noise which would come from a turbulent boundary layer on the nozzle wall is excluded. Therefore the absolute value of the computed noise level should be taken with a grain of salt. However, our aim is to find the effect of changes of geometry, so it is hoped that the *relative* values of noise level will be useful.

2.3   T5 shock tunnel with blocker

If we consider the function of the blocker to be, on the one hand, to deflect debris so that it embeds itself in the end wall, and on the other to avoid wave reflections at the shock tube axis, a reasonable blocker shape would be one that has the same diameter as the throat and a fairly large length in the region
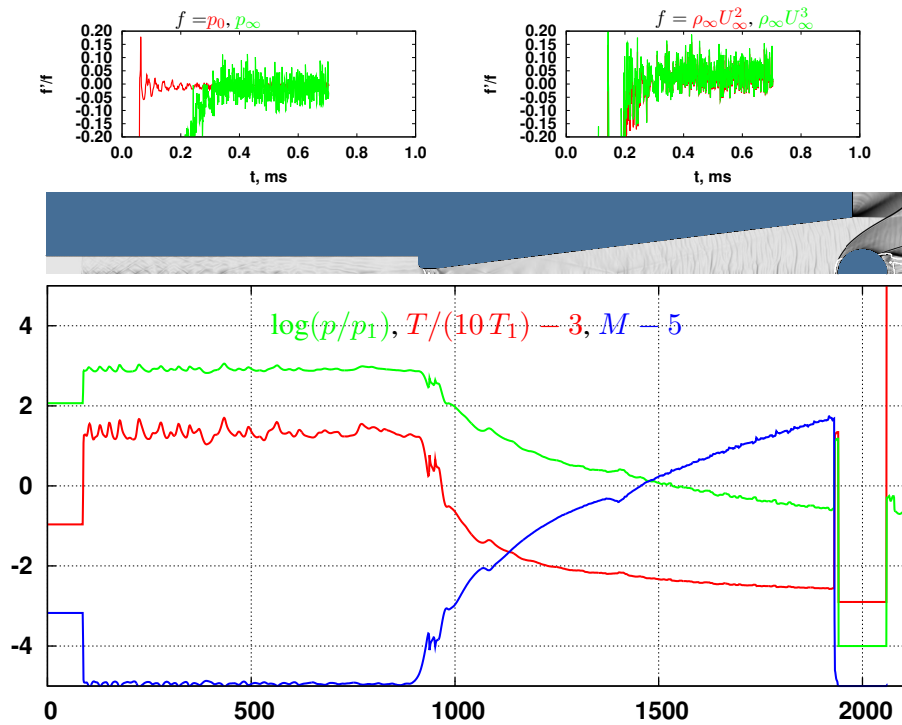
3

Figure 3: After the computation has been run for 11000 time steps with CFL number 0.8, this image results. The reflected shock is about to leave the computational domain on the left, the flow has been set up, but is quite noisy. The time traces at the top show fractional values of fluctuations of reservoir pressure p_0 measured near the shock tube wall and near the end wall, the static pressure p_∞ measured on the axis just upstream of the spherical model. At this location the right–hand time traces show $\rho_\infty u_\infty^2$ and $\rho_\infty u_\infty^3$, representative of pitot pressure and heat flux respectively.

upstream of the throat. After experimenting with a number of different shapes, the shape that emerged as fairly successful was one consisting of two slender cones pointing upstream and downstream, with the downstream cone tip just at the sonic line in the throat. The result of a computation with this blocker is shown in Fig. 4.

Even a casual inspection of Fig. 4 shows that the noise has been considerably reduced by the presence of the blocker. This is evident from the schlieren image, in which the weak shock generated at the throat and its reflections can easily be seen above the noise in the nozzle, and also from the smoother Mach number distribution, and, of course, especially from the time traces.

3 Planned Experiment

3.1 Blocker design

One of the problems associated with placing any parts in the region of the reservoir of the T5 shock tunnel is that the conditions there are extremely hostile. Temperatures and pressures are typically 9000 K and 60 MPa respectively and, for a short time between the arrival of the incident shock and the passage of the reflected shock, the flow speed is typically 3 km/s. This is also the reason why the throat material is molybdenum, which has excellent properties for the high transient heat loads encountered in the throat (up to 2 GW/m^2).

Accordingly, we made a compromise on the included angles of the conical parts of the blocker, which were increased to 30°. These conical parts will be made of molybdenum, while the remaining parts are
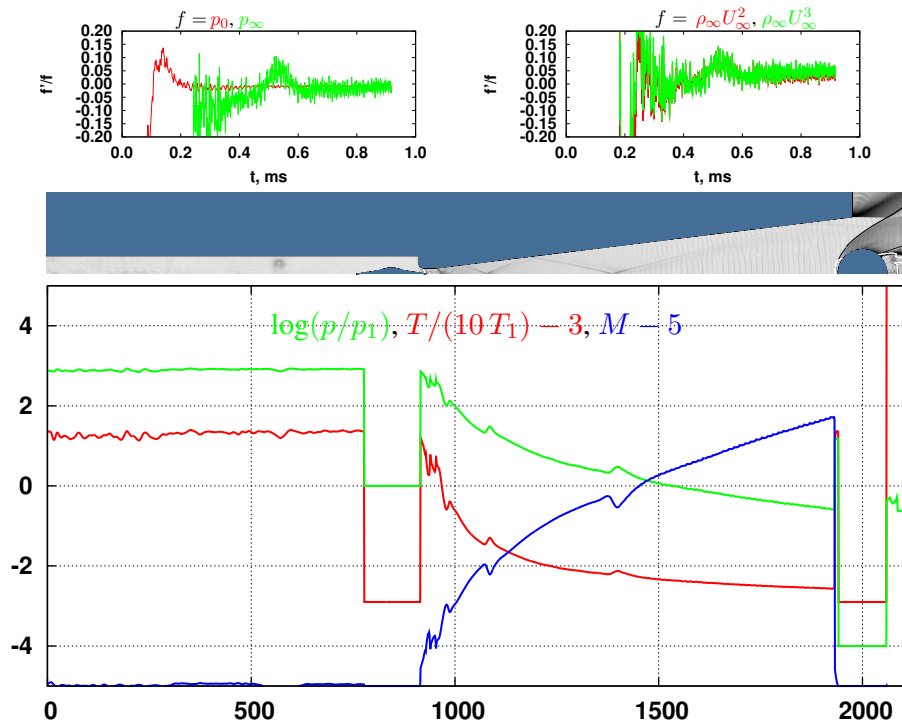
4

Figure 4: After the computation has been run for 15000 time steps with CFL number 0.8 at conditions exactly like those of Fig. 3, but with a blocker in place. It is clear that the blocker has caused a significant reduction of noise, to a level of $\pm 5\%$ in the test section variables. However, the starting time has been increased somewhat, and the vortex ring in the shock tube is prominently visible.

made of A2 tool steel electroplated with copper, in the same way as the final 50 cm of the shock tube and end wall. A perspective view of the blocker installed in the shock tube is shown in Fig. 5. The cones will be made with sharp tips initially and allowed to melt to a stable nose radius.

3.2 Noise measurement

Our interest in the noise lies particularly in the frequency range that is most strongly amplified by the second mode instability of laminar boundary layers. In the T5 shock tunnel this range is from 1 to 3 MHz. Pressure measurements are not easily possible in this range, and most optical techniques are line–of–sight integrating, so that the small structures that correspond to high frequencies are washed out by integration. However, if the focused schlieren technique is used, it is possible to resolve small structures in a small region of the flow.

In the focused schlieren technique the image of a light source is focused from a relatively large lens into the center of the test section and then with another large lens onto a knife edge as shown in Fig. 6. In order to analyze such a scheme, assume that the density distribution in a plane normal to the flow direction is

$$\rho = \rho_0 \sum_i A_i \cos ix/L \sin iy/L,$$

where ρ_0 is the average density and L is the spacing between the windows. Let the half angle of the wedge of light entering the test section be θ_1 and focus on the light ray that enters along a direction $\theta < \theta_1$.
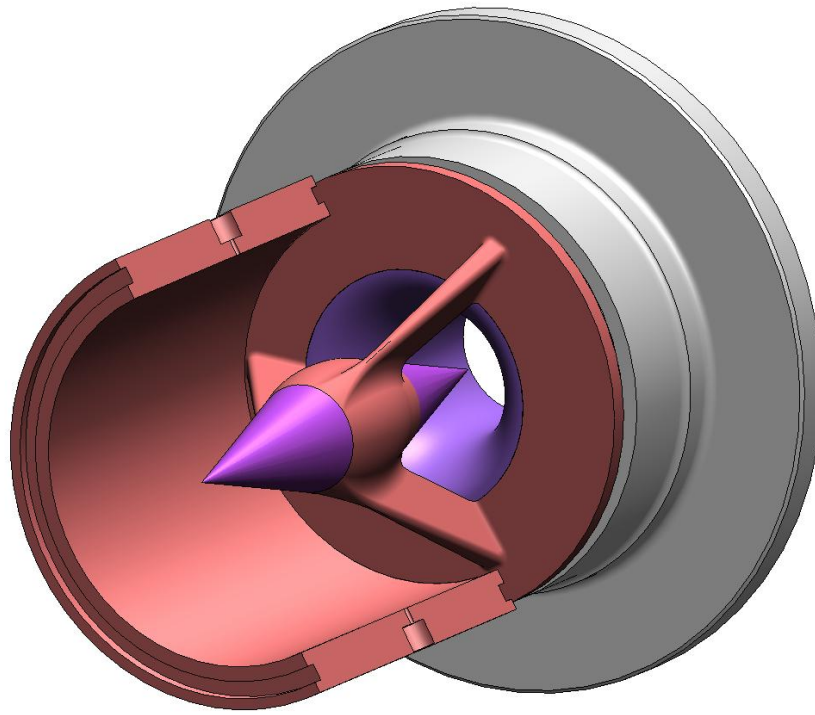
Figure 5: Perspective view of blocker installed in the end of the shock tube. Parts shown in dark red are steel with a thick coating of electroplated copper (end wall, section of shock tube sleeve, blocker support struts and centerbody of the blocker). Parts shown in magenta are molybdenum (throat and blocker cones). The sleeve section also shows the location of the two reservoir–pressure transducers.
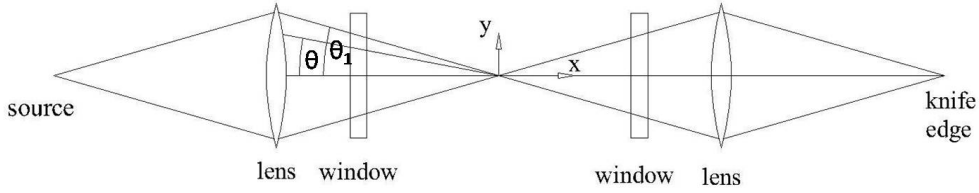

Figure 6: Sketch of optical arrangement.

3.2.1 Deflection of ray

We want to determine the deflection of the beam as it passes through the density field in the test section. The deflection is given by

$$\varepsilon = \int_{-L/2}^{L/2} \left(\frac{1}{N} \frac{\partial N}{\partial n} \right)_\theta ds,$$

where N is the refractive index of the gas and s, n are coordinates along and perpendicular to the ray. Assume θ to be sufficiently small to permit the approximation

$$\varepsilon = \int_{-L/2}^{L/2} \left(\frac{1}{N} \frac{\partial N}{\partial y} \right)_\theta dx.$$

Now introduce $N = 1 + \beta\rho/\rho_0$, where β is the Gladstone-Dale constant, which for air is approximately 0.0003. Introducing $\xi = x/L$ and $\eta = y/L$, we obtain

$$\varepsilon = \frac{2\beta L}{\rho_0} \int_0^{1/2} \left(\frac{\partial \rho}{\partial \eta} \right) d\xi, \tag{1}$$

6

or, with the approximation $\eta = \theta\xi$ for small θ,

$$\varepsilon = 2\beta L \int_0^{1/2} \sum i A_i \cos i\xi \, \cos i\theta\xi \, d\xi. \tag{2}$$

Using

$$2\cos i\xi \, \cos i\theta\xi = \cos i(1+\theta)\xi + \cos i(1-\theta)\xi$$

and integrating,

$$\varepsilon = \beta L \sum A_i \left[\frac{1}{1+\theta} \sin i(1+\theta)/2 + \frac{1}{1-\theta} \sin i(1-\theta)/2 \right]. \tag{3}$$

Assume that the light source is rectangular in shape and that the system is set up in such a way that the knife edge is parallel to the long side of the image of the light source and to the flow direction. Assume further that the deflection is small enough to prevent the image of the light source to miss the knife edge completely. These assumptions lead to the result that the change of intensity on the down-beam side of the knife edge is proportional to ε. Each beam provides a rectangular displaced image of the light source at the knife edge and makes a contribution to the change of intensity on the down-beam side. Therefore we may integrate ε over θ to obtain the total intensity change

$$\frac{\Delta I}{I_0} = 2k\beta L \int_0^{\theta_1} \sum A_i \left[\frac{1}{1+\theta} \sin i(1+\theta)/2 + \frac{1}{1-\theta} \sin i(1-\theta)/2 \right] d\theta, \tag{4}$$
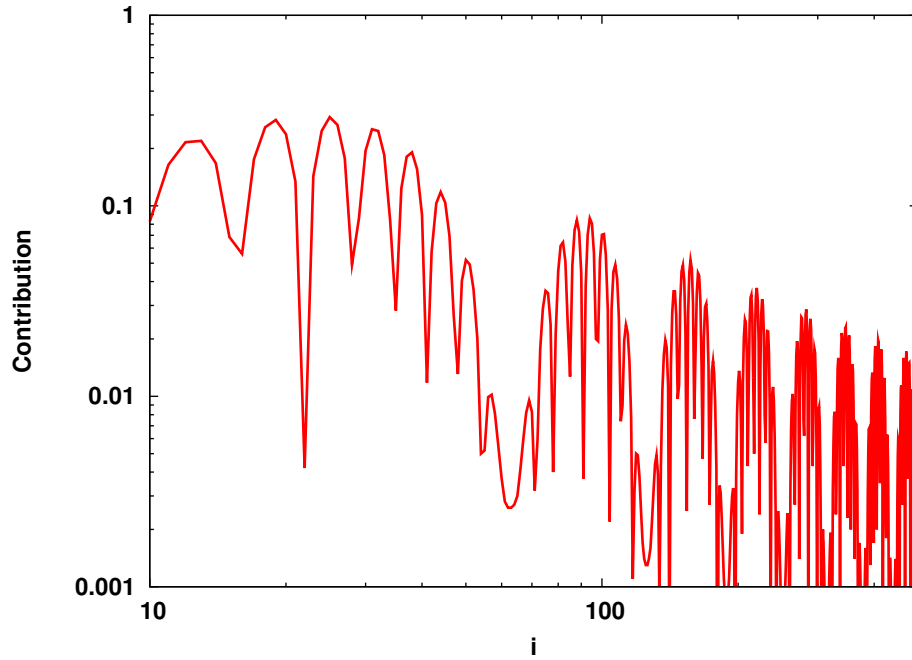
where k is a constant.

Figure 7: Contributions from the ith component to the sum for the case of $\theta_1 = 0.2$, obtained by putting all the $A_i = 1$.

Considering the integral

$$J = \int_0^{\theta_1} \frac{1}{1+\theta} \sin i(1+\theta)/2 \, d\theta,$$

we change the variable to

$$u = \frac{i(1+\theta)}{2}$$

7

to get

$$J = \int_{i/2}^{i(1+\theta_1)/2} \frac{\sin u}{u} du.$$

This allows us to write

$$\frac{\Delta I}{I_0} = 2k\beta L \sum A_i \left[\int_{i/2}^{i(1+\theta_1)/2} \frac{\sin u}{u} du + \int_{i/2}^{i(1-\theta_1)/2} \frac{\sin u}{u} du \right], \tag{5}$$

which, with the definition of $\mathrm{Si}(x)$ becomes

$$\frac{\Delta I}{I_0} = 2k\beta L \sum A_i \left[\mathrm{Si}(i(1+\theta_1)/2) - 2\mathrm{Si}(i/2) + \mathrm{Si}(i(1-\theta_1)/2) \right]. \tag{6}$$

3.2.2 Numerical example

Fig. 7 shows a plot of the magnitude of the contribution to the intensity change as a function of i for $\theta_1 = 0.2$.

This shows that the sensitivity is highly variable with i, but that, even up to $i = 500$ corresponding to structure sizes of 0.1 mm in the case of the T5 nozzle, the method has reasonable sensitivity. This scale is smaller than the size to which the light can be focused.

At the time of writing, an experimental focused schlieren system is being tested, but quantitative results have yet to be obtained.

4   Conclusions

Computations of the flow in the T5 shock tunnel show that a substantial source of noise is caused by the reflection of shock waves propagating between the shock tube axis and shock tube wall in the reservoir region of the nozzle. The sharp focusing of the wave at the axis causes very high pressure excursions. This noise can be substantially reduced by placing a center-body on the tube axis. Such a center–body is useful also in deflecting debris from the primary diaphragm rupture. A center–body design is presented. In order to measure the very high frequency noise of interest, the optical focused schlieren technique is analyzed and shown to be a feasible method of detecting small structures.

5   References

Quirk JJ (1998) Amrita — A computational facility (for CFD modelling) VKI 29th CFD Lecture Series, ISSN 0377-8312.

Hornung HG (2000) Oblique shock wave reflection from an axis of symmetry *J. Fluid Mech.* **409**, 1-12.